

# The deformation of wrinkled H<sub>2</sub>-air flames from the head on interaction with expansion waves

Hongxia Yang<sup>a</sup>, Kevin Cheevers<sup>a</sup>, Andrzej Pekalski<sup>b</sup> and Matei I. Radulescu<sup>a</sup>

<sup>a</sup> Department of Mechanical Engineering, University of Ottawa, Ottawa, Ontario, Canada

<sup>b</sup> Shell Global Solutions, Concord Business Park, Manchester, United Kingdom

## 1 Introduction

Significant pressurization during hydrogen-air explosions in open areas [1, 2], and experiments showing the deflagration-to-detonation transition of low-speed hydrogen-air flames in vented geometries [3–9] have been widely reported. It is believed that the main mechanism of flame accelerations and pressure loadings under such conditions is the turbulent mixing caused by the generation of turbulent flow fields ahead of the flames [9, 10]. A speculative theory on the origin of flame turbulization is the interaction of a flame with expansion waves generated during the sudden pressure venting. Solberg and co-workers [11] suggested that the Taylor instabilities resulting from the interaction between the flame front and the expansion waves may dominate all other mechanisms that are commonly believed to be important in governing the pressure loadings. Indeed, this same mechanism is expected to control the flame interaction with shock waves [12]. It was shown by Yang and Radulescu's work [13] that the interaction of stoichiometric cellular hydrogen-air flames with shock waves can lead to a volumetric burning rate increase by one order of magnitude for a shock wave with a modest overpressure of only approximately 3. Unfortunately, the basic physical aspects of interactions between flames and expansion waves are still not well understood.

In the present study, we addressed the flame burning rate increase from expansion waves through a series of two-dimensional direct numerical simulations. These simulations are designed to isolate the interaction of a single expansion wave with a flame, without the presence of other effects typically associated with the experimental setup such as Helmholtz bulk oscillations that are caused by wave reflections inside the experimental vessels [14], turbulence generation upon venting, etc. It is well known that planar laminar flames are unstable to hydrodynamic, thermo-diffusive, and buoyancy instabilities [15]. In lean hydrogen-air flames, it is expected that the increase in the cellular instability brought by the thermo-diffusive effects associated with low Lewis numbers significantly amplifies flame deformation. The role of low Lewis numbers in hydrogen-air flames has also been correlated with faster flame acceleration [16]. In scenarios considering the ignition of a fuel-air cloud generated by an accidental leak of hydrogen, where flame-expansion wave interactions are important, the reactive mixtures are most likely lean to stoichiometric. We thus aim to systematically investigate the controlling mechanism and parameters for these conditions. Special attention was given to the direction of the expansion wave, notably, whether it originates from the side of the fresh gas or burnt gas, the distance from the expansion wave origin to the flame, and its strength.

## 2 Numerical method and physical model

We formulate a two-dimensional problem in a rectangular domain, for which we model the problem by the reactive Navier-Stokes equations. The simulations were performed using a finite-volume code with a second-order accurate Godunov Riemann solver and adaptive mesh refinement [17, 18]. The input parameters for the model are given in table 1, calculated to fit the laminar free flame with initial conditions of 17.2 kPa, 294 K, and an equivalence ratio of  $\phi = 1.0$  and  $\phi = 0.5$  for a hydrogen-air mixture. The detailed procedure for calculating these parameters can be found in Yang and Radulescu [13].

Following [13], the cellular flame before the interaction was developed by imposing a small perturbation on a one-dimensional flame in the longitudinal direction and placed in the middle of a rectangular channel with a domain length of  $1000 L_{fs}$  and height of  $16.5 L_{fs}$ , with  $L_{fs} = \frac{K}{\rho_u S_L c_p}$  being the characteristic length scale of the flame. Once the flame sufficiently propagated to form the desired cellular flame structure, a numerical diaphragm was placed at a given distance from the cellular flame. Upon rupturing this diaphragm, which separated the domain from a low-pressure region, an expansion wave was generated with a pressure ratio between 1.6 and 2.4, as shown in Figure 1. The temperature in the low-pressure region was kept at 294K. The length of the channel was then varied within a range of  $1500L_{fs}$  and  $3000L_{fs}$  to investigate the flame evolution after the interaction.

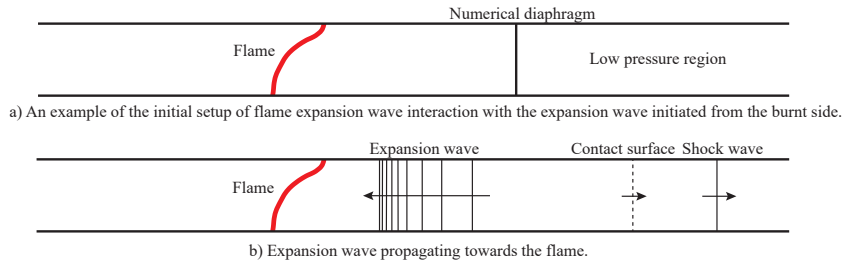


Figure 1: Sketch of the numerical set-up of the flame-expansion wave interaction.

Table 1: Thermo-chemical properties and model parameters for the hydrogen-air mixtures combustion at T=294 K and  $p_0 = 17.2$  kPa.

	$\rho_0$ (kg/m <sup>3</sup> )	$S_L$ (m/s)	$K/(\rho c_p)$ (m <sup>2</sup> /s)	$L_f$ (m)	$\gamma$	$\mu$ (pa s)
$\phi = 1.0$	0.1474	1.98	$2.60 \times 10^{-4}$	0.0034	1.4013	$1.81 \times 10^{-5}$
$\phi = 0.5$	0.1706	0.76	$2.05 \times 10^{-4}$	0.0031	1.4007	$1.82 \times 10^{-5}$
	$E_a/R$ (K <sup>-1</sup> )	$Q$ (J/kg)	$A$ (s <sup>-1</sup> )	$P_r$	$L_e$	
$\phi = 1.0$	27390	$3.00 \times 10^6$	$4.43 \times 10^{11}$	0.4655	1.0	
$\phi = 0.5$	15160	$1.72 \times 10^6$	$6.85 \times 10^9$	0.5205	0.53	

## 3 Results and discussion

### 3.1 Establishment of a cellular flame

Figure 2 shows the maximum heat release of the  $\phi = 1.0$  and  $\phi = 0.5$  flames to illustrate the evolution of the initially perturbed flame. For the flame with  $\phi = 1.0$ , the surface area and burning velocity initially increased exponentially until approximately  $35 t_{fs}$ , after which the flame stabilized to a cellular

structure with a speed of  $1.3 S_L$  and an amplitude of  $11.6L_{fs}$ . With the development of the cellular structure, the nonlinear effects became important, and the flame began to accelerate and advance.

Unlike the stoichiometric hydrogen-air flame, one notices in Figure 2 that the lean flame with  $\phi = 0.5$  developed a more wrinkled structure and had a higher overall burning velocity. The initial exponential increase in burning rate was also more intense. The formation and division of large cells with the oscillations of the flame burning rate were continuously observed until approximately  $41 t_{fs}$ . After this, the flame began to accelerate and advance. The final burning velocity was  $1.94 S_L$ , which is about 1.5 times the burning velocity of the  $\phi = 1.0$  flame.

At  $49 t_{fs}$  for the stoichiometric condition and  $28.7 t_{fs}$  for  $\phi = 0.5$ , the flames reached their maximal burning velocity. The flame structures at these times were then chosen to interact with the expansion waves initiated at their corresponding conditions.

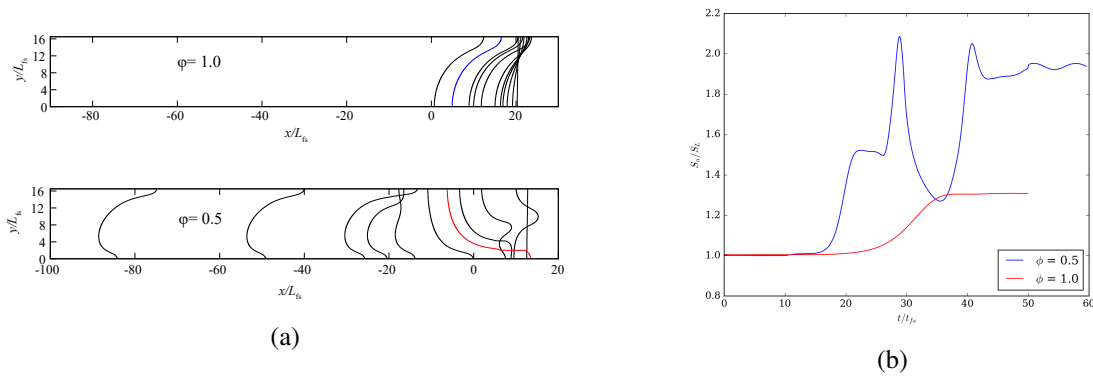


Figure 2: Time evolution of: (a) the maximum heat release contour for  $\phi = 1.0$  and  $\phi = 0.5$  flames at times  $t/t_{fs} = 0, 20, 25, 27.5, 28.7, 31, 36, 39, 41, 49$  and  $59.5$ , the red and blue curves mark the time at which the flames were chosen to interact with the expansion waves, (b) flame burning velocity.

### 3.2 Interaction of a cellular flame and an expansion wave

Figure 3(a) illustrates the detailed evolution of the interaction of a  $\phi = 0.5$  cellular flame and an expansion wave with a pressure ratio of 1.6. The expansion wave was initiated from the burnt side at a distance of  $L_0 = 141 L_{fs}$  from the flame. The first frame shows the incoming expansion wave and the flame interface before the interaction, the pressure contours mark the gradient of the expansion wave. Similar to the results of the flame interacting with the shock which originated from the unburned side in [13], the interface was reversed (2nd frame) and dragged backwards (3rd frame to the last) to the burnt gas. Certainly, the substantial thickness of the expansion wave compared to the shock wave results in a longer interaction time. From the 2nd frame, the flame developed a shape similar to funnels caused by the Richtmyer-Meshkov instability, which also agrees with the experimental results of Laviolette et al. [19]. As the funnel-shaped interface propagates further, the flame front progressively developed into a very long and narrow neck. In the last two frames, the flame burned out the gases located along the neck due to the non-linear effect caused by the baroclinic instability during the interaction, leaving only the cellular root. After this, the remaining flame front gradually decayed into another cellular flame.

Figure 3(b) shows the evolution of the flame which interacted with the expansion wave coming from the fresh side. It is obvious that the interaction also gave the flame front a mushroom shape, a flame surface area and amplitude increase, and a later burn-out of the funnel neck and the formation of a new cellular structure. However, two obvious differences can be observed compared to the expansion wave coming from the burnt side. Firstly, there is no flame front reverse. Rather, the interaction led to a direct

stretch of the flame front. Secondly, the expansion wave originating on the fresh side is more effective in deforming the flame than that originating from the burnt side.

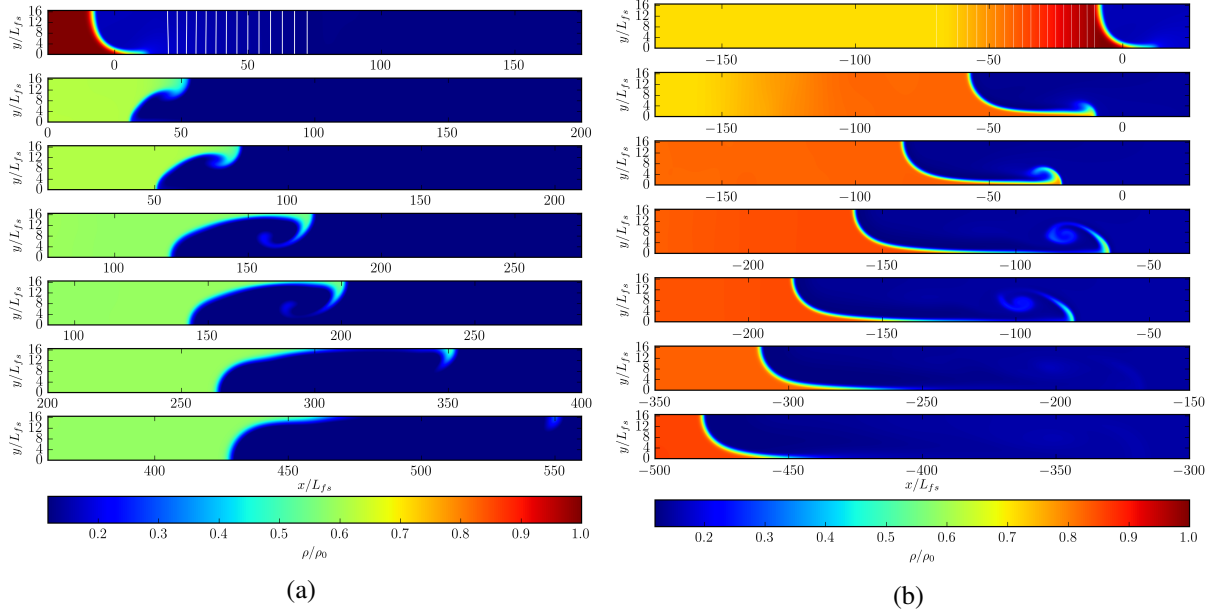


Figure 3: Density profiles illustrating the interaction of the  $\phi = 0.5$  flame and the expansion wave from the (a) burnt side and (b) fresh side of the flame at times  $t/t_{fs} = 0, 0.25, 0.35, 0.66, 0.75, 1.25$  and  $1.92$ . The white lines show the gradient of the expansion wave before interaction.

Figure 4a shows the burning velocity evolution of the flame after the interaction with the expansion wave from both the burned and unburned sides. For comparison, the burning rate evolution of the flame interacting with a shock wave with the same pressure ratio of 1.6 is also plotted. It is apparent that the highest maximum burning velocity is caused by the expansion wave generated on the fresh side, followed by the shock wave with the same pressure ratio, and then the expansion wave from the burnt side. Contrarily to the interaction with the fresh side expansion wave, the burning rates initially decreased as the shock and the burnt side expansion wave reversed the flame. The time for the flame to reach the maximum burning rate is  $0.68 t_{fs}$ ,  $0.83 t_{fs}$  and  $1.24 t_{fs}$  for the expansion wave from the fresh side, burnt side and the shock wave from the fresh side, while the burning rate increases by a factor of 7, 4.5, and 5, respectively. The lateral burn-out of the funnel neck led to a decrease in the burning velocity. It appears that although the expansion wave from the fresh side quickly increased the flame burning velocity to its maximum value, the burning velocity of the other cases stayed in the large burning rate regime for a longer duration. The overall large flame-burning rate regimes last for about 2.5 flame times.

### 3.3 Influence of flame equivalence ratio

Figure 4 compares the burning velocity of  $\phi = 0.5$  and  $\phi = 1.0$  flames following the interaction with the expansion and shock waves. It is evident that the overall burning rate evolutions for the stoichiometric flame followed the same trend as the  $\phi = 0.5$  flame for all three scenarios. Note that due to the thermo-diffusive instability, the initial burning velocity of the lean mixture is larger than that of the stoichiometric one. With an increase in flame equivalence ratio from 0.5 to 1.0, the increase in flame burning velocity is slower and less pronounced.

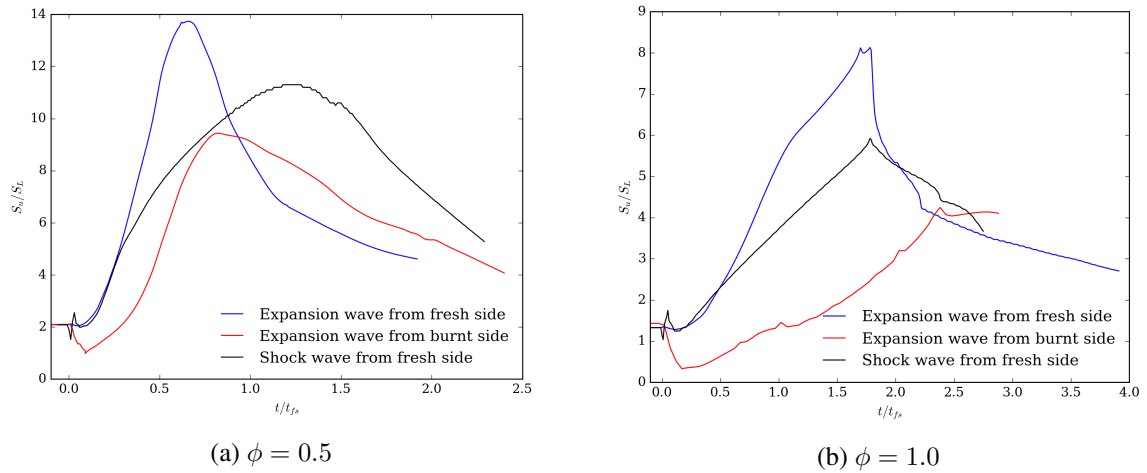


Figure 4: Time evolution of the burning velocity of  $\phi = 0.5$  and  $\phi = 1.0$  hydrogen-air flames after the interaction with expansion waves with the pressure ratio of 1.6.

### 3.4 Influence of the distance from the initiation location of the expansion wave to the flame

In this section, we isolate the problem of flame interacting with a single expansion wave generated at a distance of  $L_0$ ,  $1.5L_0$ , and  $5L_0$  from the flame. As the detailed flame evolution shown previously, Figure 5 summarizes the maximum burning velocity as a function of time for the initial conditions studied. For the flame interacting with the expansion wave initiated from the fresh side, the flame's maximum burning velocity increases with the distance from the expansion origin to the flame. The highest maximum burning velocity increases by a factor of about 6 to 9. The flame evolution after the interaction with the burnt-side expansion wave seems to be controlled by the competing effect between the pressure gradient of the expansion wave and the interaction duration time. This suggests an optimal distance between the flame and the expansion origin which is associated with the maximum burning velocity, itself a factor of 2 to 5. The time for the flame to reach the maximum burning rate is about 4 times longer for stoichiometric hydrogen-air flames than  $\phi = 0.5$  flames.

### 3.5 Influence of expansion wave strength

The simulation of stoichiometric hydrogen-air flame interacting with a stronger expansion wave initiated from the burnt side with a pressure ratio of 2.4 was also performed. It was found that following the interaction with this stronger expansion wave, the flame amplitude started to increase after the interaction whilst the flame burning velocity remained around a small near-zero value. This might suggest that a strong expansion wave may possibly quench the flame. However, whether a strong expansion wave, in reality, may quench a flame and the quenching mechanism needs further investigation.

## 4 Concluding remarks

In this study, expansion waves interacting with cellular hydrogen-air flames in a rectangular channel were systematically investigated by direct numerical simulations. The  $\phi = 0.5$  and  $\phi = 1.0$  hydrogen-air flames, which are the representative of the likely conditions for industrial accidents, interacted with expansion waves initiated from both the burned and fresh sides at varying distances from the flame, and with varied strengths. Although the lean flame has a low expansion ratio, the thermo-diffusive effects

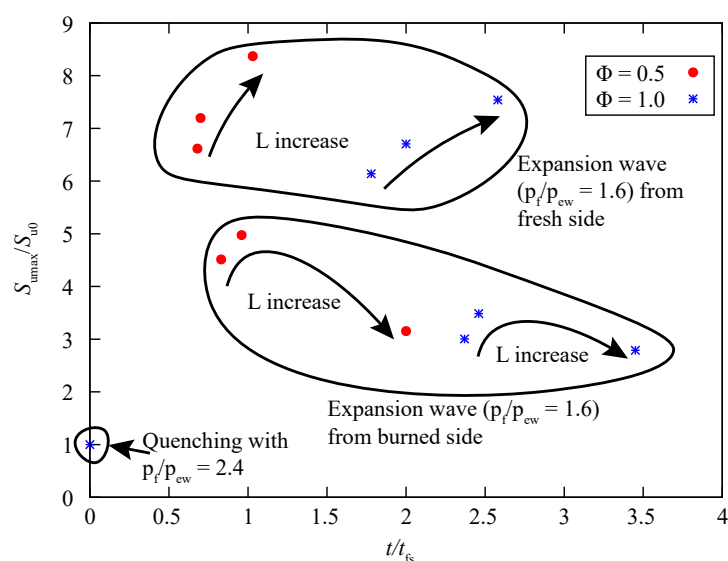


Figure 5: Summary of the maximum flame burning velocity as a function of time.

associated with low Lewis numbers caused the lean flame to be more unstable, this also led to a higher maximum burning velocity and larger growth rate following the interaction with the pressure wave. The expansion wave generated on the fresh side caused the highest increase in burning velocity by a factor of 6 to 9, whereas the expansion wave generated on the burnt side increased the burning velocity by a factor of 2 to 5. The time for the flame to reach the maximum burning rate is about 4 times longer for stoichiometric conditions than at  $\phi = 0.5$ . An optimal distance between the flame and the expansion wave origin appears when the wave is generated on the burnt side, resulting in a global maximal burning rate. This seems to be controlled by the competition between the expansion wave's pressure gradient and the interaction's duration. A strong expansion wave coming from the burned side may possibly quench the flame. Considering greater or shorter distances results in less flame enhancement stemming from the interaction. For the flame interacting with the expansion wave coming from the fresh side, the flame's maximum burning velocity increases with the initial distance separating the expansion wave and the flame. Further investigation will focus on quantifying the burning velocity evolution and rationalizing the observations with a model.

## References

- [1] M. Holt, R. J. Campbell, and M. B. Nikitin, "Fukushima nuclear disaster," 2012.
- [2] I. Mohammadfam and E. Zarei, "Safety risk modeling and major accidents analysis of hydrogen and natural gas releases: A comprehensive risk analysis framework," *International Journal of Hydrogen Energy*, vol. 40, no. 39, pp. 13 653–13 663, 2015.
- [3] M. P. Sherman, S. Tieszen, and W. B. Benedick, "Flame facility: The effect of obstacles and transverse venting on flame acceleration and transition on detonation for hydrogen-air mixtures at large scale," Nuclear Regulatory Commission, Washington, DC (USA). Div. of Systems Research, Tech. Rep., 1989.

- [4] S. Medvedev, A. Polenov, S. Khomik, and B. Gelfand, "Initiation of upstream-directed detonation induced by the venting of gaseous explosion," in *Symposium (International) on Combustion*, vol. 25, no. 1. Elsevier, 1994, pp. 73–78.
- [5] S. Dorofeev, A. Bezmelnitsin, and V. Sidorov, "Transition to detonation in vented hydrogen-air explosions," *Combustion and Flame*, vol. 103, no. 3, 1995.
- [6] G. Ciccarelli, J. Boccio, T. Ginsberg, C. Finfrock, L. Gerlach, H. Tagava, and A. Malliakos, "The effect of lateral venting on deflagration-to-detonation transition in hydrogen–air steam mixtures at various initial temperatures," *NUREG/CR e6524, BNLeNUREGe52518*, 1998.
- [7] V. Alekseev, M. Kuznetsov, Y. G. Yankin, and S. Dorofeev, "Experimental study of flame acceleration and the deflagration-to-detonation transition under conditions of transverse venting," *Journal of Loss Prevention in the Process industries*, vol. 14, no. 6, pp. 591–596, 2001.
- [8] A. Vesper, J. Grune, G. Stern, W. Breitung, and S. Dorofeev, "Flame acceleration in vented explosion tube," in *19th International Colloquium on the Dynamics of Explosions and Reactive Systems (ICDERS)*, 2003.
- [9] R. M. Kasmani, "Vented gas explosions," Ph.D. dissertation, University of Leeds, 2008.
- [10] D. Bjerketvedt, J. R. Bakke, and K. Van Wingerden, "Gas explosion handbook," *Journal of Hazardous Materials*, vol. 52, no. 1, pp. 1–150, 1997.
- [11] D. Solberg, J. Pappas, and E. Skramstad, "Observations of flame instabilities in large scale vented gas explosions," in *Symposium (International) on Combustion*, vol. 18, no. 1. Elsevier, 1981, pp. 1607–1614.
- [12] V. Kilchyk, R. Nalim, and C. Merkle, "Laminar premixed flame fuel consumption rate modulation by shocks and expansion waves," *Combustion and Flame*, vol. 158, no. 6, pp. 1140–1148, 2011.
- [13] H. Yang and M. I. Radulescu, "Dynamics of cellular flame deformation after a head-on interaction with a shock wave: reactive richtmyer–meshkov instability," *Journal of Fluid Mechanics*, vol. 923, 2021.
- [14] D. McCann, G. Thomas, and D. Edwards, "Gasdynamics of vented explosions part I: Experimental studies," *Combustion and Flame*, vol. 59, no. 3, pp. 233–250, 1985.
- [15] G. I. Sivashinsky, "Instabilities, pattern formation, and turbulence in flames," *Annual Review of Fluid Mechanics*, vol. 15, no. 1, pp. 179–199, 1983.
- [16] M. Alkhabbaz, O. Abidakun, D. Valiev, and V. Akkerman, "Impact of the Lewis number on finger flame acceleration at the early stage of burning in channels and tubes," *Physics of Fluids*, vol. 31, no. 8, p. 083606, 2019.
- [17] S. Falle, J. Giddings, K. Morton, and M. Baines, "Numerical methods for fluid dynamics 4," 1993.
- [18] B. Maxwell, A. Pekalski, and M. Radulescu, "Modelling of the transition of a turbulent shock-flame complex to detonation using the linear eddy model," *Combustion and Flame*, vol. 192, pp. 340–357, 2018.
- [19] J.-P. Lavolette, A. J. Higgins, and J. H. Lee, "Interaction between a flame and a rarefaction," in *19th International Colloquium on the Dynamics of Explosions and Reactive Systems (ICDERS)*, 2003.